

Emerging one-dimensionality from self-organization of electrons in NbSe₃

M. A. Valbuena^{1,2*}, P. Chudzinski^{3*}, S. Pons^{1,4}, S. Conejeros⁵, P. Alemany⁶, E. Canadell⁷, H. Berger¹, E. Frantzeskakis⁸, J. Avila⁸, M. C. Asensio⁸, T. Giamarchi⁹ and M. Gioni¹

¹*Institute of Physics (IPHYS), Ecole Polytechnique Federale de Lausanne (EPFL), CH-1015 Lausanne, Switzerland*

²*Catalan Institute of Nanoscience and Nanotechnology (ICN2), CSIC and The Barcelona Institute of Science and Technology, Campus UAB, Bellaterra, 08193 Barcelona, Spain*

³*Institute for Theoretical Physics, Center for Extreme Matter and Emergent Phenomena, Utrecht University, Leuvenlaan 4, 3584 CE Utrecht, The Netherlands*

⁴*Laboratoire de Physique et d'Etudes des Matériaux, 'Ecole de Physique et Chimie Industrielles' de la ville de Paris, ESPCI, PSL Research University; CNRS UMR8213; Sorbonne Universites, 'UPMC University, 10 rue Vauquelin, 75005 Paris, France*

⁵*Departamento de Química, Universidad Católica del Norte, Av. Angamos 0610, Antofagasta` 124000, Chile.*

⁶*Departament de Ciència de Materials i Química Física and Institut de Química Teòrica i Computacional (IQTCUB), Universitat de Barcelona, Martí i Franques 1, 08028 Barcelona, Spain.'*

⁷*Institut de Ciència de Materials de Barcelona (ICMAB-CSIC), Campus UAB, 08193 Bellaterra (Barcelona), Spain*

⁸*Synchrotron SOLEIL, Orme des Merisiers, Saint-Aubin-BP 48, 91192 Gif sur Yvette, France*

⁹*Department of Quantum Matter Physics, University of Geneva, 24 Quai Ernest-Ansermet, 1211 Geneva, Switzerland*

Materials where the electron filling is close to commensurability provide one of the great challenges in materials science. Several proposals of unconventional orderings, where the electronic liquid self-organizes into components with distinct properties, were recently put for-

ward, in particular in cuprates¹⁻⁶ and pnictides^{7,8} where electronic nematic orders have been observed. The electrons' self-organization is expected to yield complex intra and inter unit cell patterns, and a reduction of dimensionality. Nevertheless, an unambiguous experimental proof of such complex orders, namely the direct observation of distinct dispersions, is still missing. Here we report a Nano Angle Resolved Photoemission Spectroscopy (NanoARPES) study of NbSe₃, a material that has been considered a paradigm of charge order. The new data (Fig.1) invalidate the canonical picture of imperfect nesting⁹ and reveals the emergence of a novel order. The electrons' self-organization uncovers the one-dimensional (1D) physics hidden in a material which naively should be the most 3D of all columnar chalcogenides.

NbSe₃ undergoes two successive charge density waves (CDW) transitions¹⁰ at $T_{C1} = 145$ K and $T_{C2} = 59$ K, affecting electrons on distinct columns¹¹⁻¹⁴ of its crystal structure shown in Fig.2(a). The charge ordering is not strong enough to remove the entire Fermi surface^{10,15}, and metallic conduction is observed even below T_{CDW2} . The nature of the gapless states has proven to be quite elusive, with several proposals^{9,15-17} for the location of pockets within the Brillouin zone. In this paper we exploit NanoARPES with ultra-high lateral resolution and polarization control to probe these gapless states and to address the mechanism behind their formation (details on the experimental technique are available in Suppl. Mat.). NbSe₃ crystals grow in the form of very thin whiskers that assemble in bundles. The nanometric lateral resolution of the Antares beamline k -microscope proved crucial to select the best homogeneous areas in well-cleaved monodomain single crystals.

Figure 1 illustrates NanoARPES data collected with two photon polarizations along the ΓZ

(chains) direction in the low temperature phase ($T < 59$ K), where the sample experiences both CDW₁ and CDW₂. For s-polarization (Fig 1(a)), perpendicular to the b axis of the sample, we observe 3 parabolic bands, labelled A1⁺, C2 and A3⁺, near the Fermi energy (E_F), similar to previous ARPES investigations^{9,18}. The effect of the CDWs is revealed by multiple gaps at E_F : in band C2 from CDW₁, and in bands A1⁺ and A3⁺ from CDW₂. From an analysis of spectra extracted from the energy-momentum map we estimate the gap values $\Delta_{C2} = \Delta_1 = 84$ meV and $\Delta_{A1^+} = \Delta_{A3^+} = \Delta_2 = 20$ meV, consistent with Ref.⁹. A gap in A3⁺ at k_{F2} ($E_{gap} \approx 2\Delta_1$ around $E_B = 0.18$ eV) and the apparent continuity of the folded bands C2 and A3⁺ indicate an hybridization of these two bands driven by the CDW₁ potential. Data taken with p-polarization (Fig.1(d)) reveal different and unexpected features. Two linearly dispersing bands (labelled A1⁻ and A3⁻) now cross E_F with no CDW-related gaps. These bands do not correspond to any of the spectral features observed with s-polarization for the same area of the single crystal. Such dramatic polarization dependence suggests that different types of carriers are present, and that they are separable by some selection rule.

As a first step to understand the experimental findings we performed advanced (GGA+U) DFT calculations. The inclusion of a local interaction term U allows us to better differentiate Nb atoms with formally different oxidation states. The results of the calculation are shown in Fig.2(b), with further details in the Suppl. Mat. They confirm that the A1⁺, A3⁺ and C2 bands observed with s-polarization can be associated with crystal columns A and C. The calculated k_F values are in good agreement with the measured data. The two bands labelled C are degenerate near E_F as in the NanoARPES experiment where they appear as a single band, C2, implying a very small hybridization within a pair of C columns. Although the calculated bands crossing E_F mainly derive

from d orbitals of a given Nb atom, the d weight is never more than 50%, a rather different situation from e.g. transition metal oxides. This is a manifestation of the covalent character of the Nb-Se bonds and implies that the electron clouds are not locked on the Nb d orbitals but potentially can be deformed when an extra potential from CDWs develops. The band dispersion has a quasi1D character, but the anisotropy is only moderate: the calculated bandwidth is $W_b = 2.5$ eV along the b axis and up to 250 meV along perpendicular directions. The previously proposed band structures^{9,16,17} hold also when local correlations are included, but U causes vertical shifts of the bands labelled B and Se. Namely, band B is now located just above E_F , a result compatible with recent scanning tunneling microscopy measurements¹⁴ where a significant spectral weight appears just above E_F . This may enhance inter-band backscattering, a process that controls the CDW_2 transition described below.

If the electrons could move within the crystal coherently in all directions, then the symmetry *planes* would be those of the $P2_1/m$ monoclinic space group of NbSe₃, parallel to the ac plane. Since the scattering plane in our NanoARPES experiment is perpendicular to these symmetry planes no definite selection rule should apply¹⁹. Identical dispersions should be observed for the two polarizations²⁰, in stark contrast with the measured data. The paradox is solved if correlations inhibit the coherent motion of electrons within the ac plane, endowing NbSe₃ with a strong onedimensional character. This implies that the standard nesting scenario

¹ The electrons are incoherent in the ac plane at high energies due to the hopping anisotropy (see Suppl. Mat. for calculation of an effective anisotropy)

for CDW formation, based on a warped 2D Fermi surface, must be abandoned and that a new description must be found.

To do so we first consider the bands C2 which, in our GGA+U calculations, are degenerate and nearly commensurate, and hence act as a doublet of 1D chains, prone to a Peierls distortion. Indeed the C2 dispersion is clearly backfolded, an effect of the CDW₁ with

$$\vec{q}_1 = (0, 0.241b^*, 0),$$

for which a charge distortion is known to be located mostly^{11,12,14} on columns C. Its 1D character manifests itself in an anomalously large²¹ ratio $\frac{\Delta_1}{T_{c1}} = 6.7$. The CDW₁ transition partitions the rest of the electronic liquid into 1D sub-systems¹ located on quartets of A+B columns (charge is predominantly on column A with some delocalization on column B). Each pair of A columns acts as a two-leg ladder system, where the competition of several internal interactions governs the physics²²⁻²⁵. An organization in the ac plane with a chessboard pattern (Fig.3(c)), which is a natural choice from the interactions viewpoint, allows to resolve the competition. Such pattern naturally yields the CDW₂ periodicity $q_2^\perp = (\frac{a^*}{2}, \frac{c^*}{2})$, which is hard to justify in a standard nesting scenario. Moreover this *ansatz* directly solves several experimental riddles: the band doubling into A1(3)⁺ and A1(3)⁻ and their tiny splitting, the number of electrons that remain ungapped, and the presence of gapless carriers close to the Γ point. For instance, dispersions A1(3)⁺ and

² In the following we indicate by $\psi_{Ai}(r)$, the orbital that is a real space representation of an eigenstate corresponding to a DFT band Ai^+ .

A1(3)⁻ correspond to newly formed bonding(+) / anti-bonding(-) states between adjacent quartets illustrated in Fig3 (b), that we shall call $\gamma_{1(3)}^{\pm}$.

The above self-organization is governed by a dimerization along the c-axis. The driving force comes from a change in shape of the emerging eigen-orbitals $\psi_{\gamma_{\pm 1,3}}(r)$ (of the states $\gamma_{1,3}^{\pm}$), which in turn changes the character of the electron-electron (e-e) interactions. For the emergent bonding state $\gamma_{1,3}^+$ the charge density of the constituent states $\psi_{A3}(r)$ (or $\psi_{A1}(r)$) extends towards column C (see Fig3(b)). While for $\psi_{A1,3}(r)$ there is only the long-range (Coulomb-type) interaction with CDW₁, which decays when the exchanged momentum increases, the emergent bonding states $\psi_{\gamma_{\pm 1,3}}(r)$ overlap more strongly with $\psi_C(r)$ and exchange processes become more likely. Hence the nature of the e-e interactions between carriers on column A and CDW₁ changes from long-range Coulomb type for $\psi_{A1,3}(r)$ to a more local (Hubbard) type for $\psi_{\gamma_{\pm 1,3}}(r)$. The scattering channel with large momentum exchange is accordingly enhanced. For the γ_3^+ state, the enhanced backscattering allows for a significant re-hybridization with a gapped band C2 (see Fig.1), an effect that has been noticed before⁹. The band structure of the $\gamma_{1,3}^+$ states is illustrated in Fig.3(a). The re-hybridization enhances e-e interactions with exchanged momentum close to $\sim q_1$, as shown by arrows. Since $\sim q_1$ is very close to $\vec{k}_{F1} + \vec{k}_{F3}$, the momentum exchanged in the inter-band backscattering processes, these processes are enhanced and can open a gap in the spectrum of the two-leg ladder (see Fig.3(a)). Thus, the emergent bonding states γ^+ are gapped and CDW₂, with $\vec{q}_2 = \vec{k}_{F1} + \vec{k}_{F3}$, has an intrinsically many-body origin.

Implications of our *ansatz* can be immediately tested. Firstly, since electrons move incoherently within the ac plane, an effective symmetry plane for the 1D system consisting of a quartet of A+B columns must: i) be perpendicular to the c-axis, ii) contain the b-axis, and iii) cross the middle of the quartet. The scattering plane σ_l fulfils these conditions and thus the dipole selection rules emerge. Therefore the observed polarization dependence is a good indicator of the existence of a 1D regime. The bonding states γ^+ are by construction delocalized towards column C, hence they involve p-Se σ -hybridization on the short link (green line in Fig.2). These states are anti-symmetric with respect to the σ_l plane (see Fig.3b) and hence are expected to appear in s-polarization, in agreement with the experiment. A π -bond component on the short bond, required to keep the total density close to the DFT solution, can be absorbed within the anti-bonding state γ^- . These states are symmetric (vs σ_l) and hence visible in p-polarization. Moreover, since they are localized mostly in the core of the quartet and interact weakly with CDW_1 , they are expected to be gapless. These are the new states uncovered in p-polarization.

Another implication is that the gapless states $\gamma_{1,3}^-$ should behave in accordance with the predictions of the 1D Tomonaga-Luttinger liquid (TLL) theory [Ref.^{26,27}]. The momentum-integrated spectrum should exhibit a power-law dependence with a characteristic non-universal exponent α . This behavior is compatible with the data with $\alpha = 0.24$ (see Fig.4(e)). Moreover, the k -resolved spectra should exhibit several modes (for a standard TLL there are two modes corresponding to spinon and holon, but for a ladder up to four modes are possible²⁷) each with its own dispersion relation. Fits to the line shapes of energy- and momentum-distribution curves from our NanoARPES data in p-polarization expose that both the $A1^-$ and the $A3^-$ bands contain

separate linear and parabolic dispersions, outlined with different symbols ("h" for holon and "s" for spinon) in Fig.4, that converge at $k_{F1,3}$. Note that these modes do not overlap with any features observed in the opposite polarization Fig.4(b). This strongly suggests a different behavior than in a Fermi liquid, in which only one velocity can appear. *All* signatures illustrated in Fig.4 are at least compatible with the TLL behavior.

In conclusion, NbSe₃ is the first material where electrons' self-organization into nano-sized emergent eigenstates with a strong 1D character is revealed by means of NanoARPES. This observation provide an insight into the CDW formation and self-differentiation mechanisms which are fully captured by our model resulting in two sets of states with distinct dispersions, one of which is gapped and the other one has TLL properties. The polarization dependence of NanoARPES allows these (orbitally distinct) states to be selectively probed. These results open the way to new experiments searching for the emergence of hidden 1D dimensional states in strongly correlated materials.

Acknowledgements

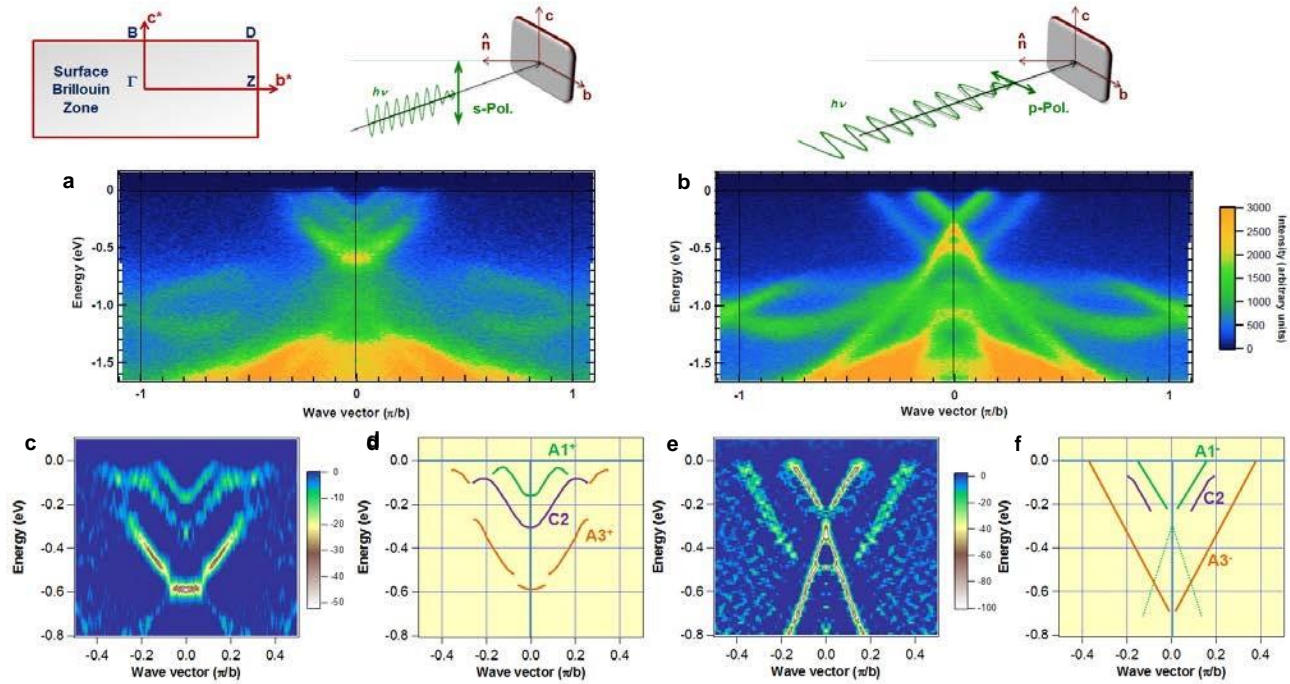


Figure 1: ARPES intensity maps taken in the Γb^* direction with photons of 100eV of two different polarizations. (a) s-polarization (b) ARPES p-polarization. Insets : experimental geometry and surface Brillouin zone. *s*-polarization is perpendicular to the long axis of NbSe₃ crystalline whiskers (i.e. perpendicular to the *b* axis). *p*-polarization has a component along the long axis of the whisker (i.e. along the *b* axis) and a component out of the plane. (c) Curvature procedure applied to the ARPES intensity map (a) (d) schematic of the band diagram recorded in (a) showing two parabolic bands associated to columns A (A1⁺ & A3⁺) and one parabolic band associated to columns C (C2). (e) Curvature procedure applied to the ARPES intensity map (b). Extrapolating the dispersions of the bands to E_F yields $k_{F1} = 0.14\pi/b$; $k_{F2} = 0.22\pi/b$ and $k_{F3} = 0.37\pi/b$. (f) schematic of the band diagram recorded in (b) showing two new linear bands labeled A1⁻ & A3⁻ and a weak contribution of band C2.

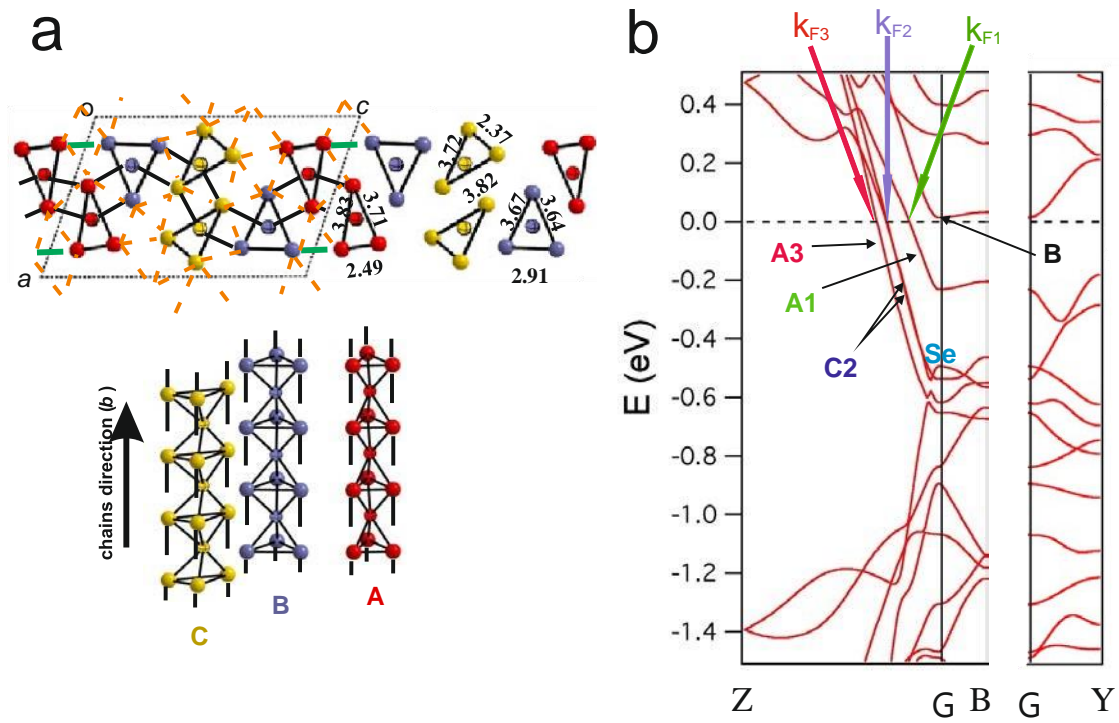


Figure 2: Crystal structure and DFT calculations. (a) Crystal structure of NbSe₃ built out of prismatic columns of three types, hereafter labeled column A-C. Bottom: View along the 1D chains (along the \tilde{b} axis): Three types of columns are indicated in red (A), blue (B) and yellow (C).

Top: (ac) plane cross-section. Green (orange) dashed lines indicate strong (weak) Se...Se intercolumnar contacts. (b) Theoretical DFT GGA band calculations including finite $U = 4$ eV. Each band is indicated by the dominant orbital component. The bands can be associated with experimental counterparts presented in Fig.1 by comparison of the Fermi wave vectors. See supplementary material online for further calculation details.

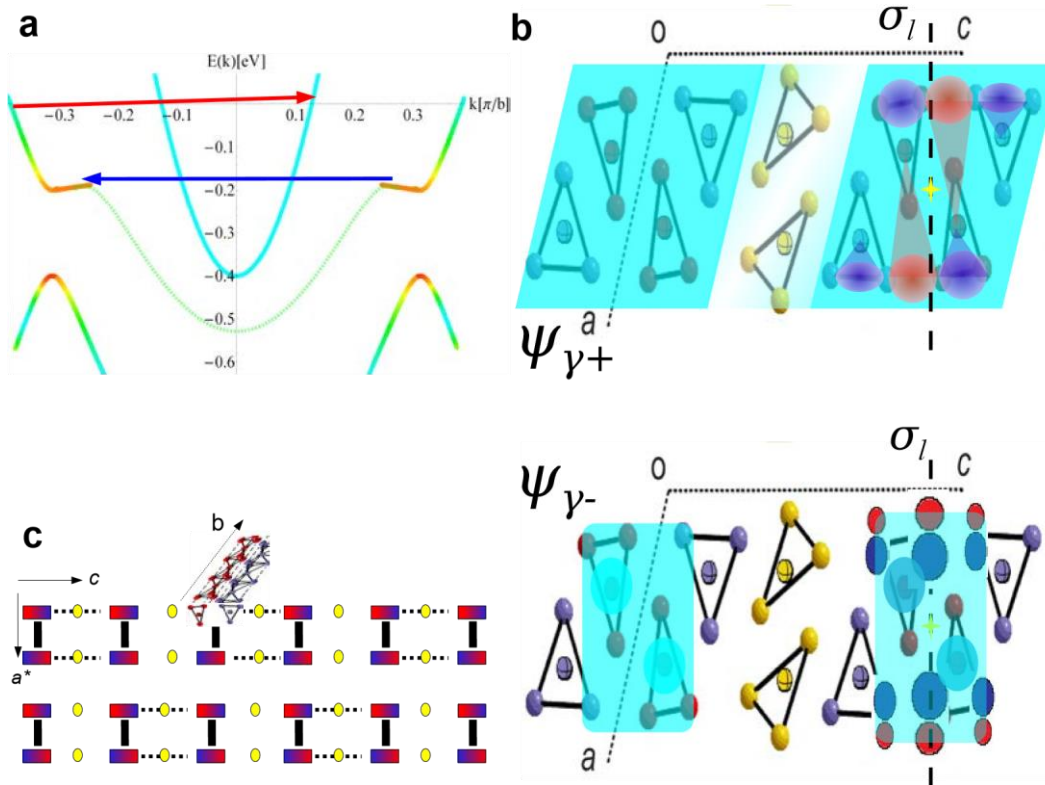


Figure 3: Electrons self-organization model. (a) Model band structure of re-hybridized γ^+ states shows a proximity of an inter-band $A3^+ \rightarrow A1^+$ back-scattering (red-arrows) to a periodicity of CDW₁ q_1 (blue arrow). The color scale encodes band curvature: when approaching red one approaches the van Hove singularity, where scattering processes are enhanced. (b) Bonding γ^+ (upper panel) and anti-bonding γ^- (lower panel) eigen-orbitals emerging from a perpendicular dimerization between two neighboring unit cells of a basic crystal structure. Distinct wavefunctions are shown to have a different spatial extension. The amplitude is indicated by the strength of turquoise shading. Red and blue color indicates the phase of the involved p -orbitals. The orientation of a p -orbital determines the direction in which the resulting ψ_γ orbital will be extended. The two wavefunctions are quite different, yielding *even* character on the bottom panel and *odd* character on the top panel (vs. the σ_l plane indicated by the dashed line). (c) the cross section on a - c plane showing schematically the perpendicular dimerization and emergent self-organization. Yellow dots represent col. C where the “high energy physics”, formation of CDW₁ takes place. Pairs of red-blue rectangles linked by thick black line are doublets of A+B columns. Bands A1 and A3 are bonding anti-bonding bonds formed on the black line. The perpendicular dimerization is

indicated by the dashed black lines and it corresponds to bonding ($A1^+$ and $A3^+$) and anti-bonding ($A1^-$ and $A3^-$) combinations (with a tiny energy split).

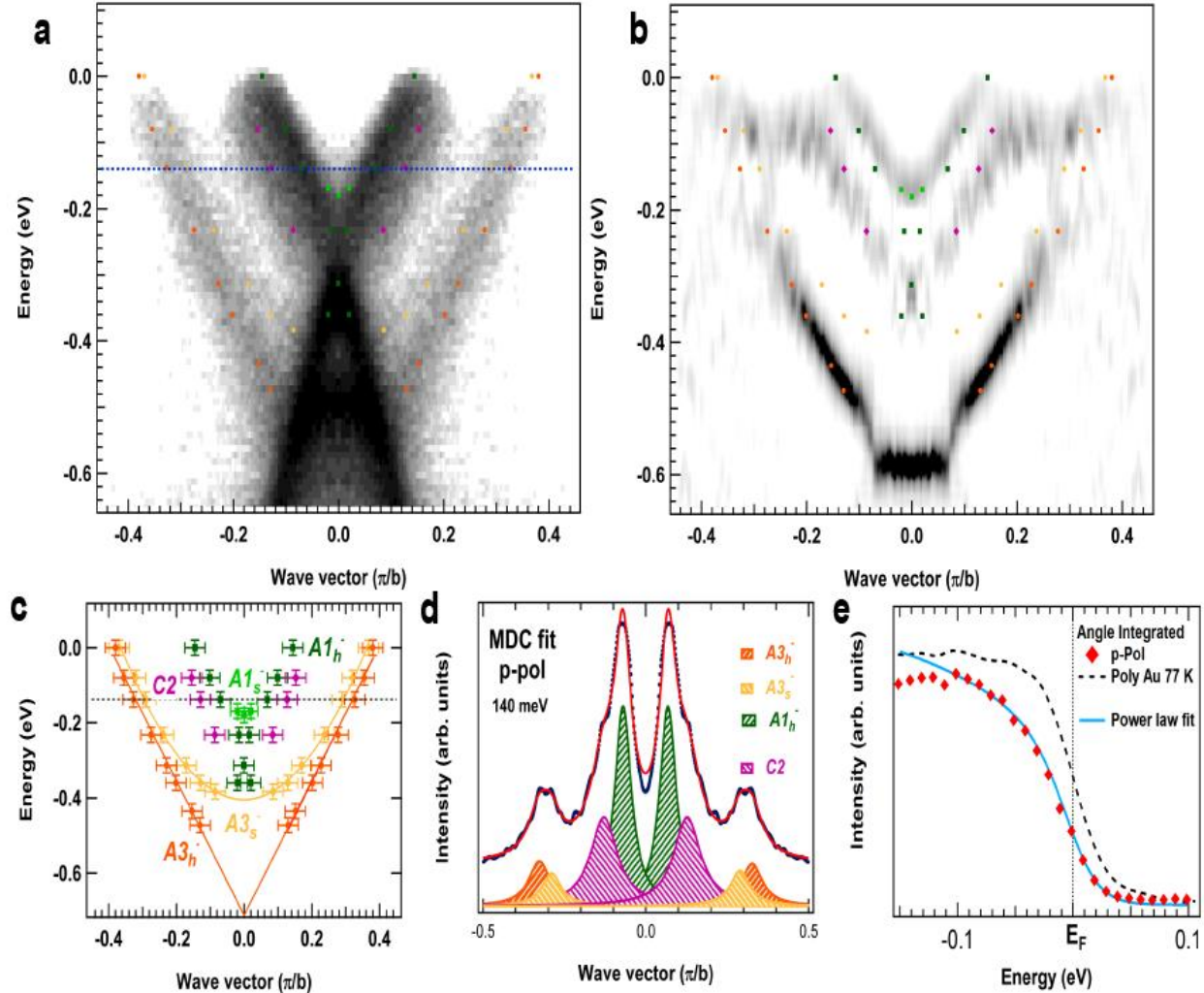


Figure 4: Signatures of 1D physics within the electronic states in NbSe₃:(a) Spectral intensity close to the Fermi level recorded with *p*polarization. Please note: observed extensions of $A1^-_h$ beyond the Dirac point at $E_{D1} = -0.25$ eV), that were puzzling for DFT, are remarkably similar to the TLL-“shadow bands”²⁸; (b) Comparison of observed data-points with the curvature image obtained with *s*-polarization. ; (c) Result of the fit of the spectral intensity measured with *p*-polarization as shown in panel(a). The fit evidences two component for each band *A*, $A1^-_s$ and $A1^-_h$, $A3^-_s$ and $A3^-_h$. Please note: the two double dispersions $A1^-_h, A3^-_h$ are geometrically similar – the ratios $E_{D1,3}/E_{B1,3}$ are equal (as expected for a two leg ladder). (d) example of MDC fit which has allowed us to find data points along the white dashed line in panel A (also indicated as dashed line in panel C); (e) Integrated intensity showing a power-law like vanishing of the density of states, compatible with a TLL behavior, fit following Ref.^{29,30}.

The work at Lausanne and Geneva is supported by the Swiss NSF. M.A.V. acknowledges financial support from Spanish MICIN Postdoctoral Mobility Program. SP acknowledges C'NANO Ile-de-France, DIM NanoK, for the support of the Nanospecs project. Work in Spain was supported by a MINECO (Grants FIS2015-64886-C5-4-P and CTQ2015-64579-C3-3-P), Generalitat de Catalunya (2014SGR301) and XRQTC. E.C. and M.A.V. acknowledge support from MINECO through the Severo Ochoa Centers of Excellence Program under Grants SEV-2015-0496 and SEV2013-0295. SC gratefully acknowledges the Becas Chile program (CONICYT PAI/INDUSTRIA 72090772) for a doctoral grant at the Universitat de Barcelona. Synchrotron SOLEIL is supported by the Centre National de la Recherche Scientifique (CNRS) and the Commissariat a l'Energie Atomique et aux energies Alternatives (CEA).

Author Contributions

H.B. grew the single crystal samples; M.A.V., S.P. and M.G. designed the experiment; M.A.V., S.P., J.A. and E.F. performed the experiments assisted by M.C.A.; M.A.V., and S.P. and J.A. analyzed the NanoARPES data; S.C, P.A. and E.C. performed the DFT calculations; P.C. and T.G. elaborated the theoretical model; P.C., S.P., E.C. and M.G. wrote the paper with comments from all co-authors.

1. Lawler, M. J. *et al.* Intra-unit-cell electronic nematicity of the high-Tc copper-oxide pseudogap states. *Nature* 466, 347–351 (2010).
2. Mesaros, A. *et al.* Topological defects coupling smectic modulations to intraunit-cell nematicity in cuprates. *Science* 333, 426–430 (2011). URL <http://www.sciencemag.org/content/333/6041/426.abstract>. <http://www.sciencemag.org/content/333/6041/426.full.pdf>.
3. da Silva Neto, E. H. *et al.* Charge ordering in the electron-doped superconductor $\text{Nd}_{2x}\text{Ce}_x\text{CuO}_4$. *Science* 347, 282–285 (2015). URL <http://www.sciencemag.org/content/347/6219/282.abstract>. <http://www.sciencemag.org/content/347/6219/282.full.pdf>.
4. Ghiringhelli, G. *et al.* Long-range incommensurate charge fluctuations in $(\text{Y,Nd})\text{Ba}_2\text{Cu}_3\text{O}_{6+x}$. *Science* 337, 821–825 (2012). URL <http://www.sciencemag.org/content/337/6096/821.abstract>. <http://www.sciencemag.org/content/337/6096/821.full.pdf>.
5. Comin, R. *et al.* Broken translational and rotational symmetry via charge stripe order in underdoped $\text{YBa}_2\text{Cu}_3\text{O}_{6+y}$. *Science* 347, 1335–1339 (2015). URL <http://www.sciencemag.org/content/347/6228/1335.abstract>. <http://www.sciencemag.org/content/347/6228/1335.full.pdf>.
6. Kivelson, S. A. & Fradkin, E. High-temperature superconductivity: Ineluctable complexity. *Nat.Phys.* 8, 864–866 (2010).
7. Chuang, T.-M. *et al.* Nematic electronic structure in the parent state of the iron-based superconductor $\text{Ca}(\text{Fe}_{1-x}\text{Co}_x)_2\text{As}_2$. *Science* 327, 181–184 (2010). URL <http://www.sciencemag.org/content/327/5962/181.abstract>. <http://www.sciencemag.org/content/327/5962/181.full.pdf>.
8. Glasbrenner, J. K. *et al.* Effect of magnetic frustration on nematicity and superconductivity in iron chalcogenides. *Nat.Phys.* 2015/08/24/online (2015).
9. Schafer, J. *et al.* High-temperature symmetry breaking in the electronic band structure of the quasi-one-dimensional solid NbSe_3 . *Phys. Rev. Lett.* 87, 196403 (2001). URL <http://link.aps.org/doi/10.1103/PhysRevLett.87.196403>.

10. Monceau, P., Ong, N. P., Portis, A. M., Meerschaut, A. & Rouxel, J. Electric field breakdown of charge-density-wave–induced anomalies in NbSe₃. *Phys. Rev. Lett.* 37, 602–606 (1976). URL <http://link.aps.org/doi/10.1103/PhysRevLett.37.602>.
11. Pouget, J.-P., Moret, R., Meerchaud, A., Guemas, L. & Rouxel, J. X-ray observation of 1-d precursor effects in NbSe₃ and new diffuse scattering features in FeNb₃Se₁₀. *J. Phys. (France) Colloq.* 44, 1729 (1983).
12. van Smaalen, S. *et al.* Determination of the structural distortions corresponding to the q^1 - and q^2 -type modulations in niobium triselenide NbSe₃. *Phys. Rev. B* 45, 3103–3106 (1992). URL <http://link.aps.org/doi/10.1103/PhysRevB.45.3103>.
13. Wada, S., Aoki, R. & Fujita, O. Nmr study of the electronic state and peierls transitions in NbSe₃. *Journal of Physics F: Metal Physics* 14, 1515 (1984). URL <http://stacks.iop.org/0305-4608/14/i=6/a=019>.
14. Brun, C., Wang, Z.-Z. & Monceau, P. Scanning tunneling microscopy at the NbSe₃ surface: Evidence for interaction between q_1 and q_2 charge density waves in the pinned regime. *Phys. Rev. B* 80, 045423 (2009). URL <http://link.aps.org/doi/10.1103/PhysRevB.80.045423>.
15. Perucchi, A., Degiorgi, L. & Thorne, R. E. Optical investigation of the charge-density-wave phase transitions in NbSe₃. *Phys. Rev. B* 69, 195114 (2004).
16. Shima, N. Band structure of NbSe₃. *Journal of the Physical Society of Japan* 52, 578–586 (1983). URL <http://dx.doi.org/10.1143/JPSJ.52.578>.
<http://dx.doi.org/10.1143/JPSJ.52.578>.
17. Canadell, E. *et al.* Comparison of the electronic structures of layered transition-metal trichalcogenides tantalum triselenide, tantalum trisulfide and niobium triselenide. *Inorganic Chemistry* 29, 1401–1407 (1990).
18. Schafer, J. *et al.* Unusual spectral behavior of charge-density waves with imperfect nesting in a quasi-one-dimensional metal. *Phys. Rev. Lett.* 91, 066401 (2003). URL <http://link.aps.org/doi/10.1103/PhysRevLett.91.066401>.
19. Hermanson, J. Final-state symmetry and polarization effects in angle-resolved photoemission spectroscopy. *Solid State Communications* 22, 9–11 (1977).
20. Mesot, J. *et al.* Determination of the fermi surface in high- T_c superconductors by angle-resolved photoemission spectroscopy. *Phys. Rev. B* 63, 224516 (2001). URL <http://link.aps.org/doi/10.1103/PhysRevB.63.224516>.
21. Fournel, A., Sorbier, J. P., Konczykowski, M. & Monceau, P. Measurement of the charge-density-wave gap of NbSe₃ from tunnel-junction spectra. *Phys. Rev. Lett.* 57, 2199–2202 (1986). URL <http://link.aps.org/doi/10.1103/PhysRevLett.57.2199>.

22. Dagotto, E., Riera, J. & Scalapino, D. Superconductivity in ladders and coupled planes. *Phys. Rev. B* 45, 5744–5747 (1992).
URL <http://link.aps.org/doi/10.1103/PhysRevB.45.5744>.
23. Tsunetsugu, H., Troyer, M. & Rice, T. M. Pairing and excitation spectrum in doped $t - J$ ladders. *Phys. Rev. B* 49, 16078–16081 (1994). URL <http://link.aps.org/doi/10.1103/PhysRevB.49.16078>.
24. Schulz, H. J. Phases of two coupled Luttinger liquids. *Phys. Rev. B* 53, R2959–R2962 (1996). URL <http://link.aps.org/doi/10.1103/PhysRevB.53.R2959>.
25. Abbamonte, P. *et al.* Crystallization of charge holes in the spin ladder of $\text{Sr}_{14}\text{Cu}_{24}\text{O}_{41}$. *Nature* 431, 1078 (2005).
26. Haldane, F. D. M. Effective harmonic-fluid approach to low-energy properties of one-dimensional quantum fluids. *Phys. Rev. Lett.* 47, 1840–1843 (1981). URL <http://link.aps.org/doi/10.1103/PhysRevLett.47.1840>.
27. Giamarchi, T. *Quantum Physics in One Dimension* (Oxford University Press, Oxford, 2004).
28. Schmidt, T. L., Imambekov, A. & Glazman, L. I. Spin-charge separation in one-dimensional Fermion systems beyond Luttinger liquid theory. *Phys. Rev. B* 82, 245104 (2010). URL <http://link.aps.org/doi/10.1103/PhysRevB.82.245104>.
29. Fisher, M. P. A. & Dorsey, A. T. Dissipative quantum tunneling in a biased double-well system at finite temperatures. *Phys. Rev. Lett.* 54, 1609–1612 (1985). URL <http://link.aps.org/doi/10.1103/PhysRevLett.54.1609>.
30. Bockrath, M. *et al.* Luttinger-liquid behaviour in carbon nanotubes. *Nature* 397, 598–601 (1999).